Electronic Supplementary Material (ESI) for New Journal of Chemistry.

Supporting Information

A new multi-analyte fluorogenic sensor for efficient detection of Al^{3+} and Zn^{2+} ions based on ESIPT and CHEF feature

Lakshman Patra, Sangita Das, Saswati Gharami, Krishnendu Aich andTapan Kumar Mondal*

Department of Chemistry, Jadavpur University, Kolkata-700 032, India.

E-mail: tapank.mondal@jadavpuruniversity.in

Visible colour change

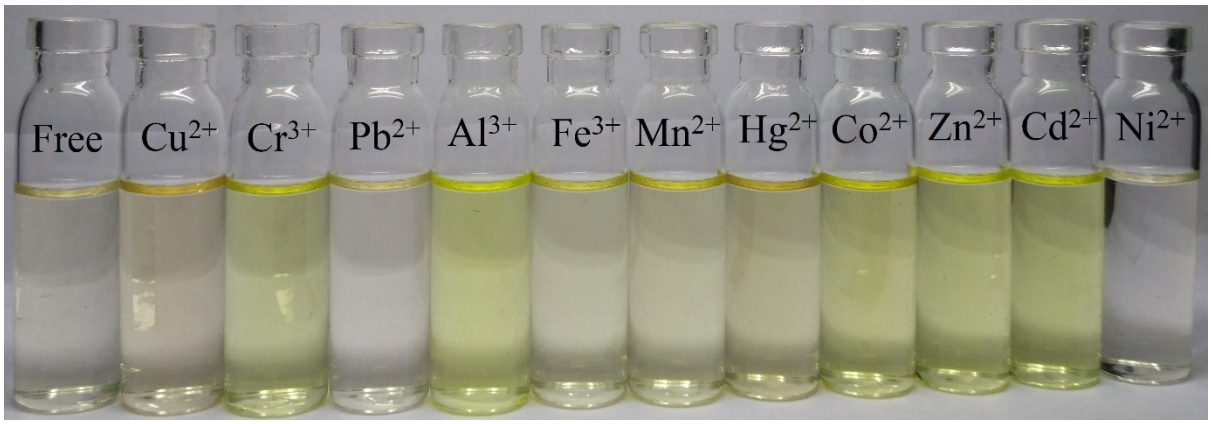

Fig. S1:Visible colour change of H_2L under ambient light, upon addition of different anions as stated.

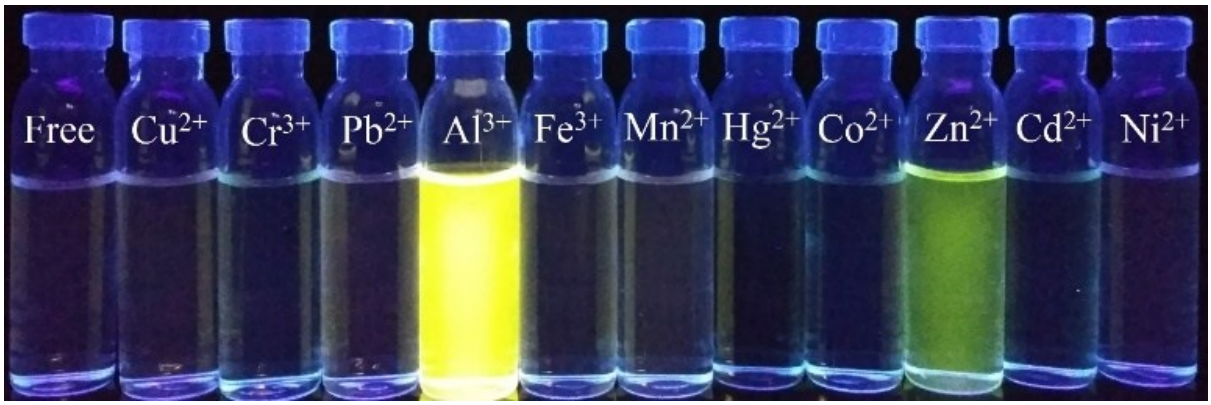

Fig. S2: Fluorescence changes of the receptor upon addition of stated anions after irradiation under UV light.

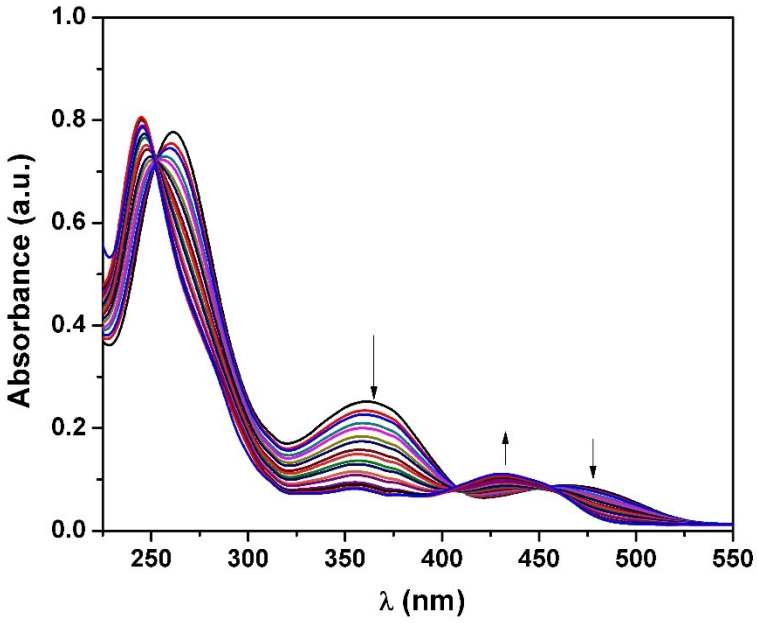

Fig. S3: Change in UV-Vis spectrum of **H_2L** (20 μM) upon gradual addition of Al^{3+}(40μM)in CH_3OH/H_2O (4/1, v/v, pH = 7.2).

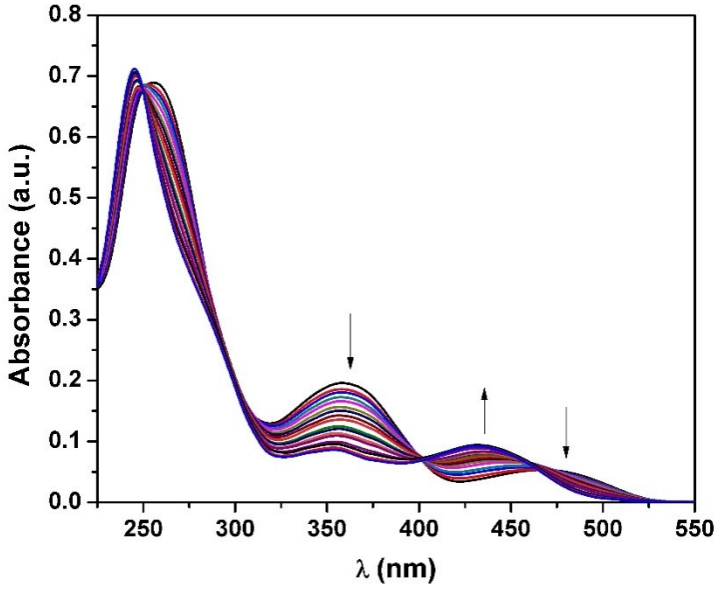

Fig. S4: Change in UV-Vis spectrum of **H_2L** (20 μM) upon gradual addition of Zn^{2+}(40μM)in CH_3OH/H_2O (4/1, v/v, pH = 7.2).

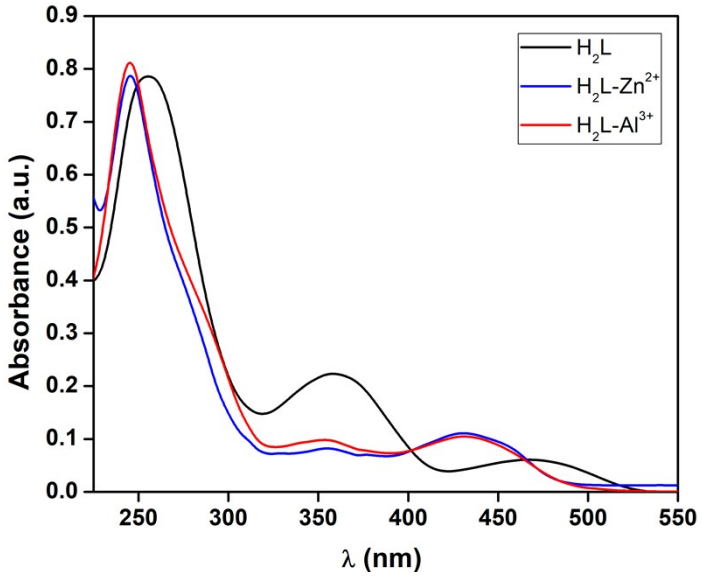

Fig. S5: Change in absorption spectrum of H_2L (20 μM) upon complexation with Al^{3+} and Zn^{2+}(40 μM) in CH_3OH/H_2O (4/1, v/v, pH = 7.2) solution.

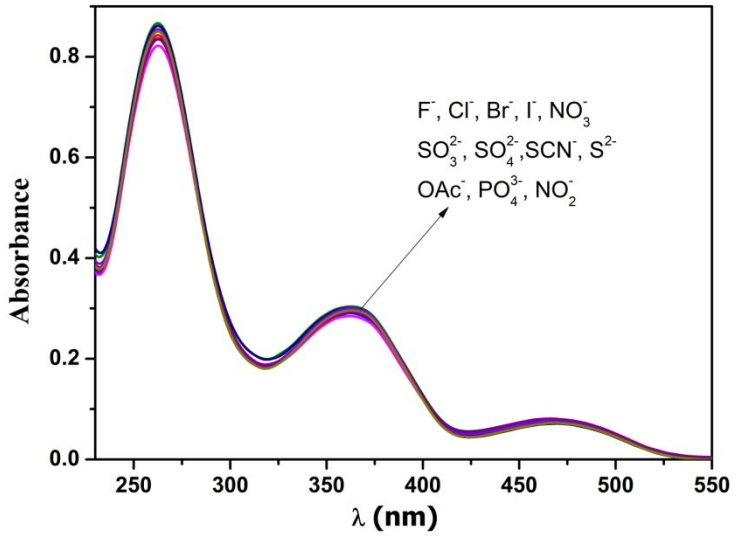

Fig. S6: Change in absorption spectrum of H_2L (20 μM) upon addition of different anions (40 μM) in CH_3OH/H_2O (4/1, v/v, pH = 7.2) solution.

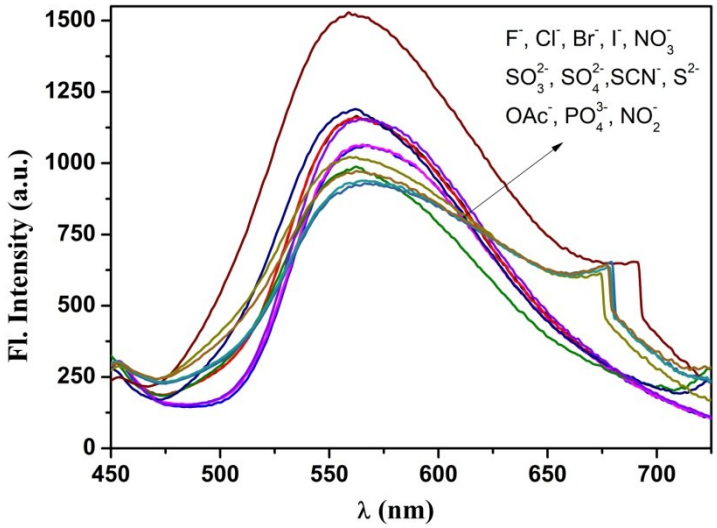

Fig. S7: Change in emission spectrum of H2L (20 μM) upon addition of different anions (40 μM) in CH3OH/H2O (4/1, v/v, pH = 7.2) solution.

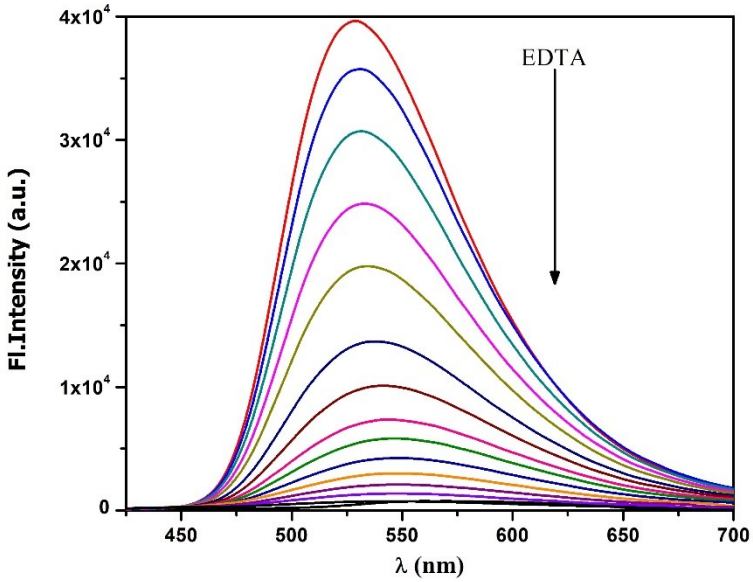

Fig. S8: Change in emission spectrum of H_2L–Zn2+ complex(20 μM) upon gradual addition of EDTA solution(40 μM) in CH_3OH/H_2O (4/1, v/v, pH = 7.2) solution, λ_{ex} = 400 nm.

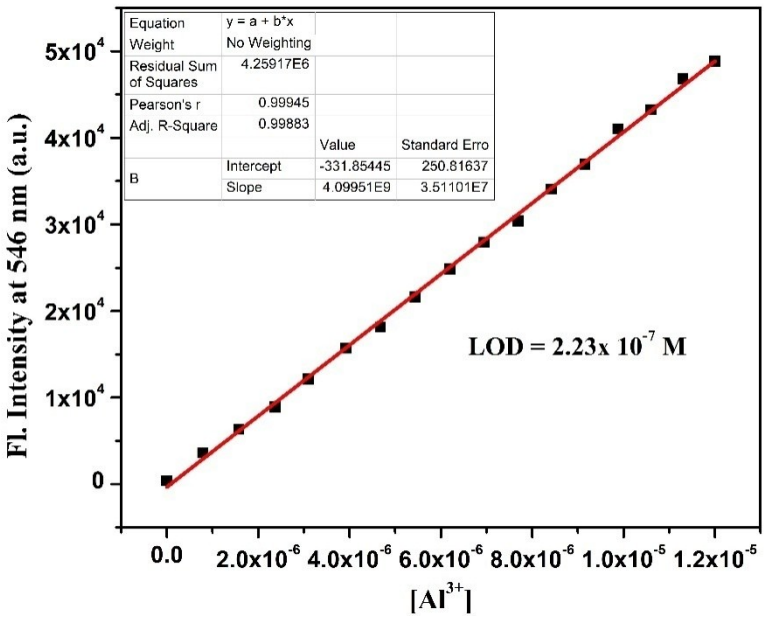

Fig. S9: Linear response curve of **H_2L** at 546 nm depending on the Al^{3+}concentration.

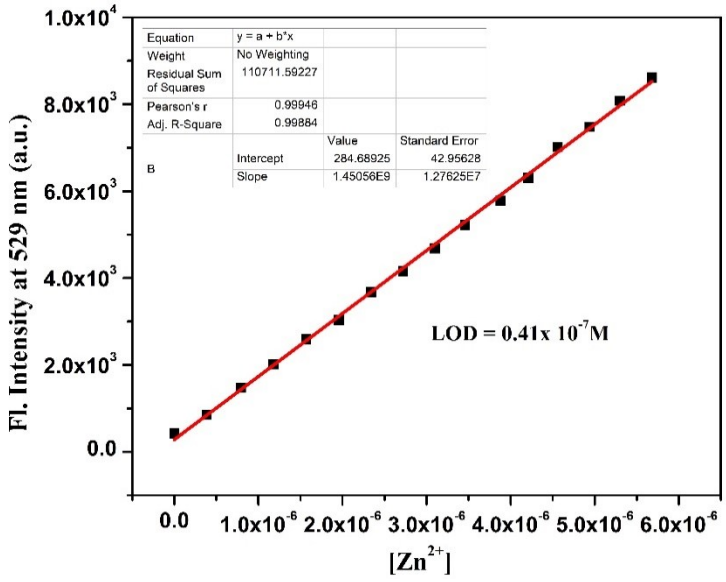

Fig. S10: Linear response curve of **H_2L** at 529 nm depending on the Zn^{2+}concentration.

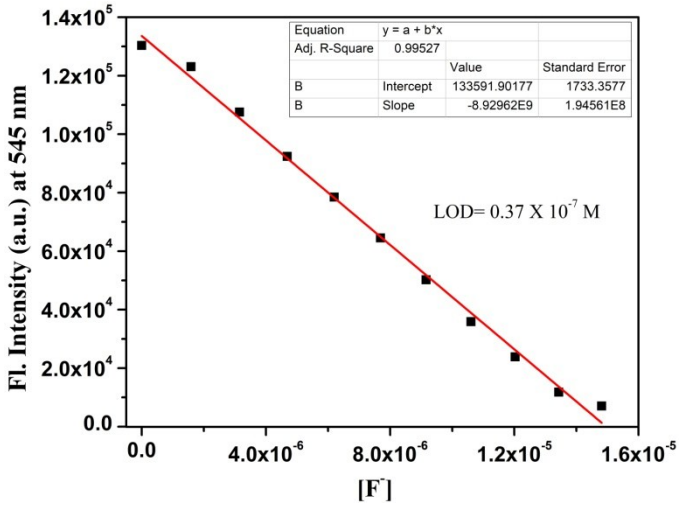

Fig. S11: Linear response curve of $\mathbf{H_2L\text{-}Al^{3+}}$ adduct solution at 546 nm depending on the F^- concentration.

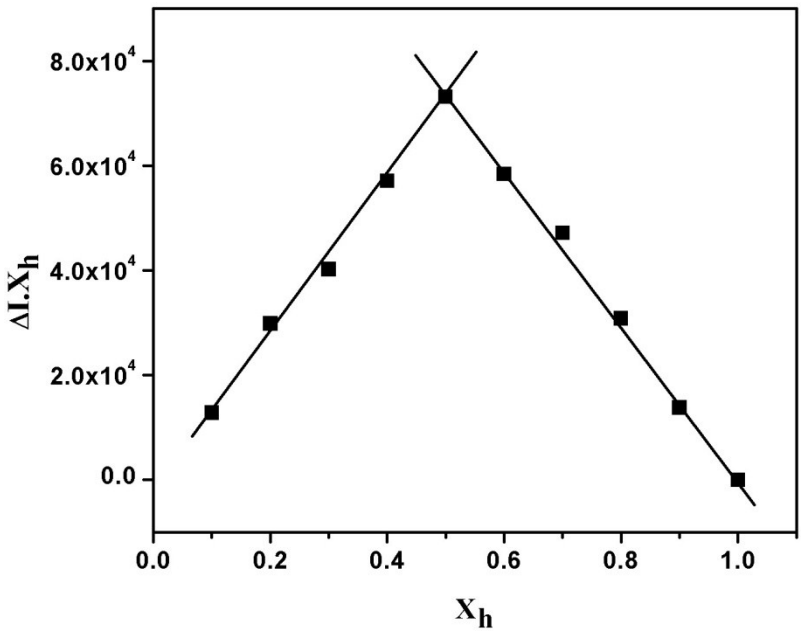

Fig. S12: Job's plot for $H_2L\text{-}Al^{3+}$ complex formation using fluoroscence emission titration experiment (λ_{ex} = 400 nm); where X_h is the mole fraction of the host and ΔI indicates the change of emission at 545 nm.

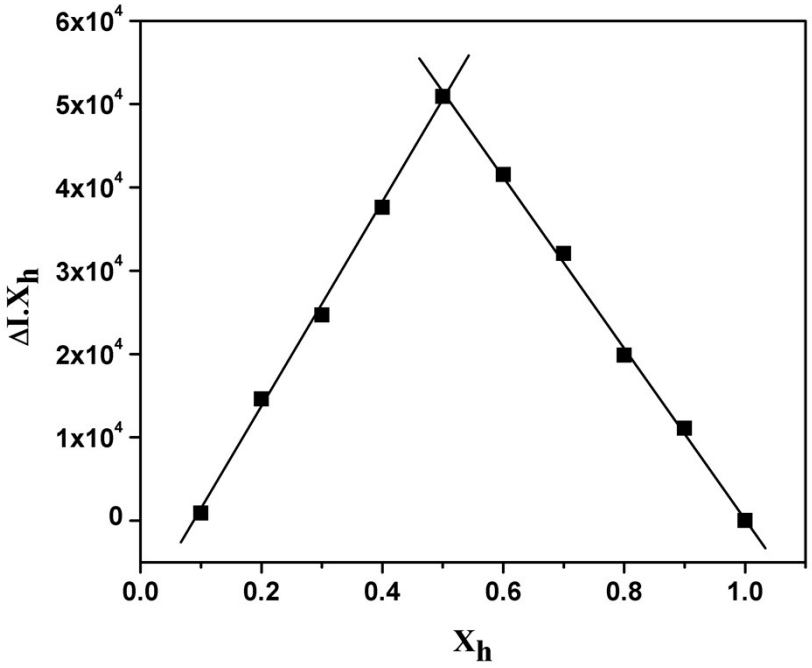

Fig. S13: Job's plot for H_2L-Zn^{2+} complex formation using fluoroscence emission titration experiment (λ_{ex} = 400 nm); where X_h is the mole fraction of the host and ΔI indicates the change of emission at 529 nm.

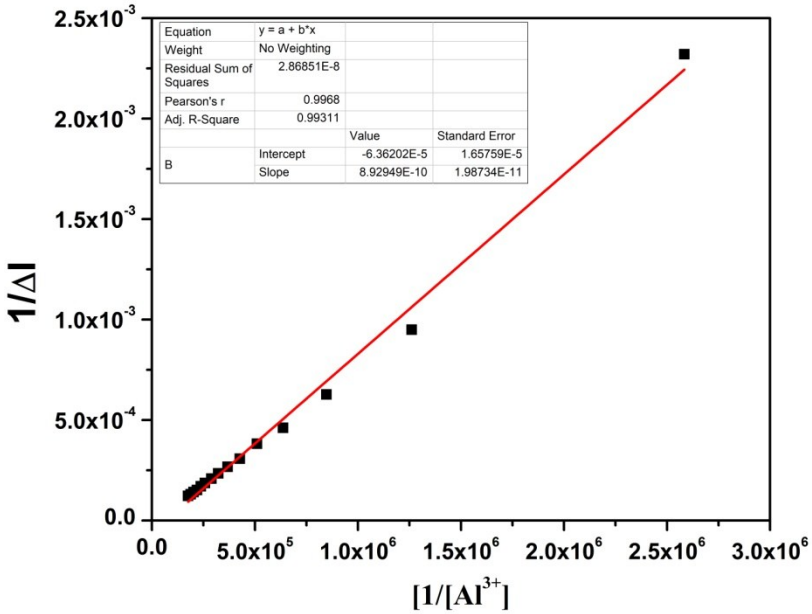

Fig. S14: Benesi–Hildebrand plot from fluorescence titration data of receptor (20 μM) with Al^{3+}.

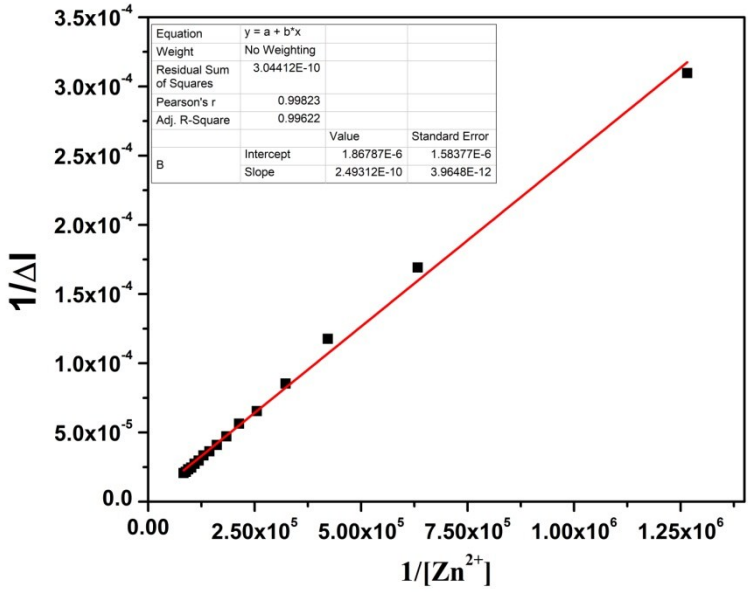

Fig. S15: Benesi–Hildebrand plot from fluorescence titration data of receptor (10 μM) with Zn^{2+}.

Table S1: Fluorescence lifetime data

CH_3OH (solvent)	Quantum yield *(φ)*	τ (ns)	k_r ($10^8 \times s^{-1}$)	k_{nr} ($10^8 \times s^{-1}$)
H_2L	0.00215	1.60	0.013	6.23
H_2L-Al^{3+}	0.212	5.02	0.422	1.57
H_2L-Zn^{2+}	0.041	2.30	0.178	4.16

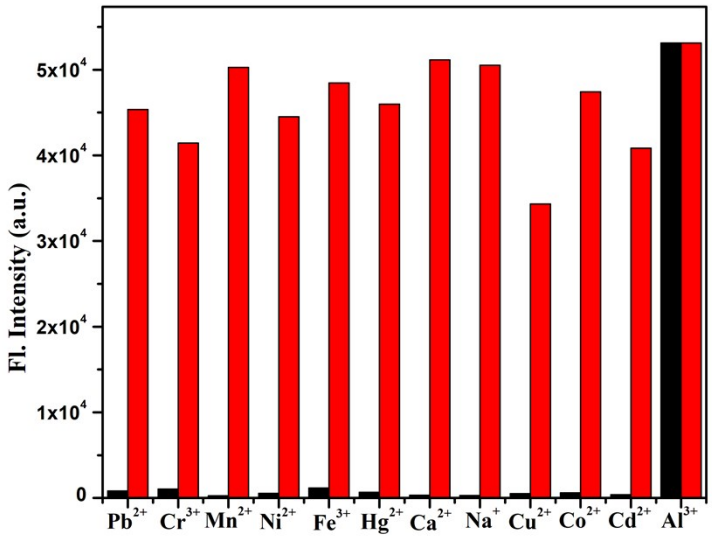

Fig. S16: Fluorescence intensity response of **H_2L**(20 μM) upon the addition of Al^{3+} in the presence of interference cations in CH_3OH/H_2O (4/1, v/v).

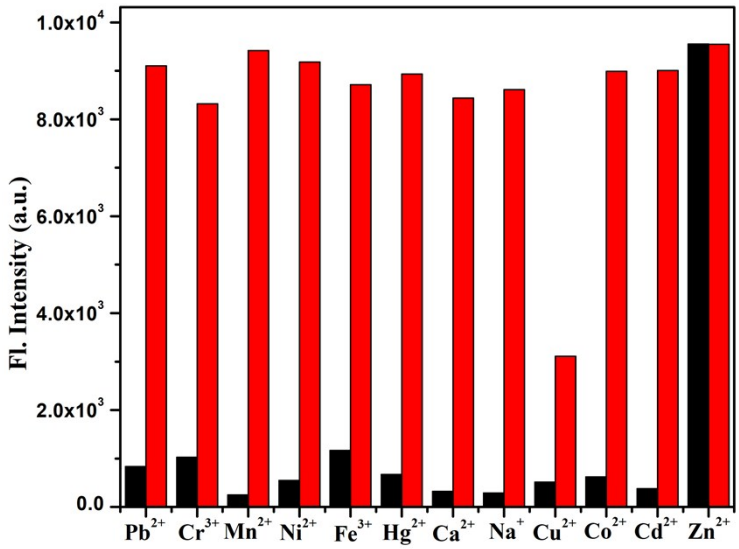

Fig. S17: Fluorescence intensity response of **H_2L**(20 μM) upon the addition of Zn^{2+} in the presence of interference anions in CH_3OH/H_2O (4/1, v/v).

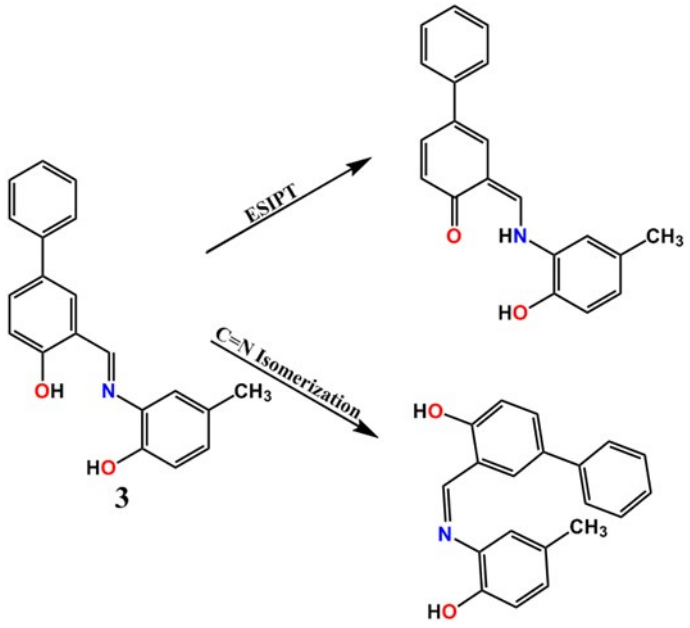

Fig. S18: Probable ESIPT effect and isomerisation process; cause of very weak emission of free receptor.

^{1}H NMR, IR and HRMS spectra

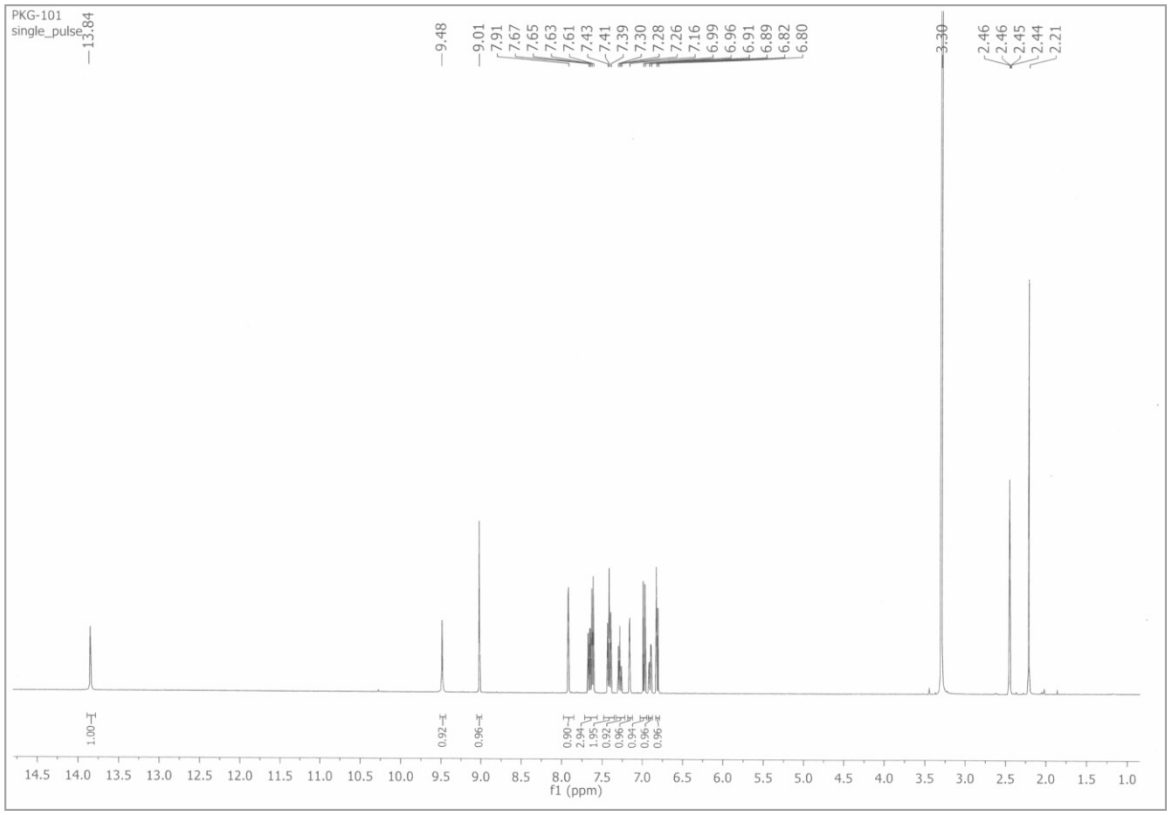

Fig. S19: ^{1}H NMR (400 MH_Z) spectrum of **H_2L** in DMSO-d6.

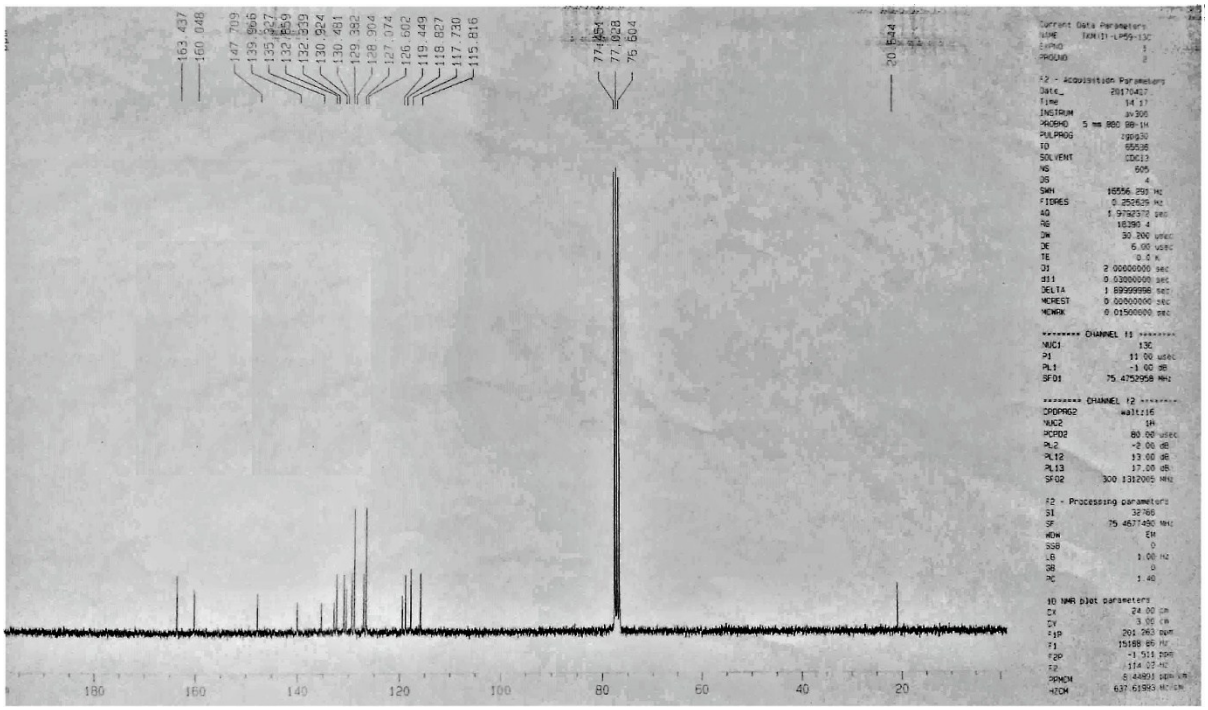

Fig. S20:^{13}C NMR (300 MH_Z) spectrum of **H_2L** in DMSO-d6.

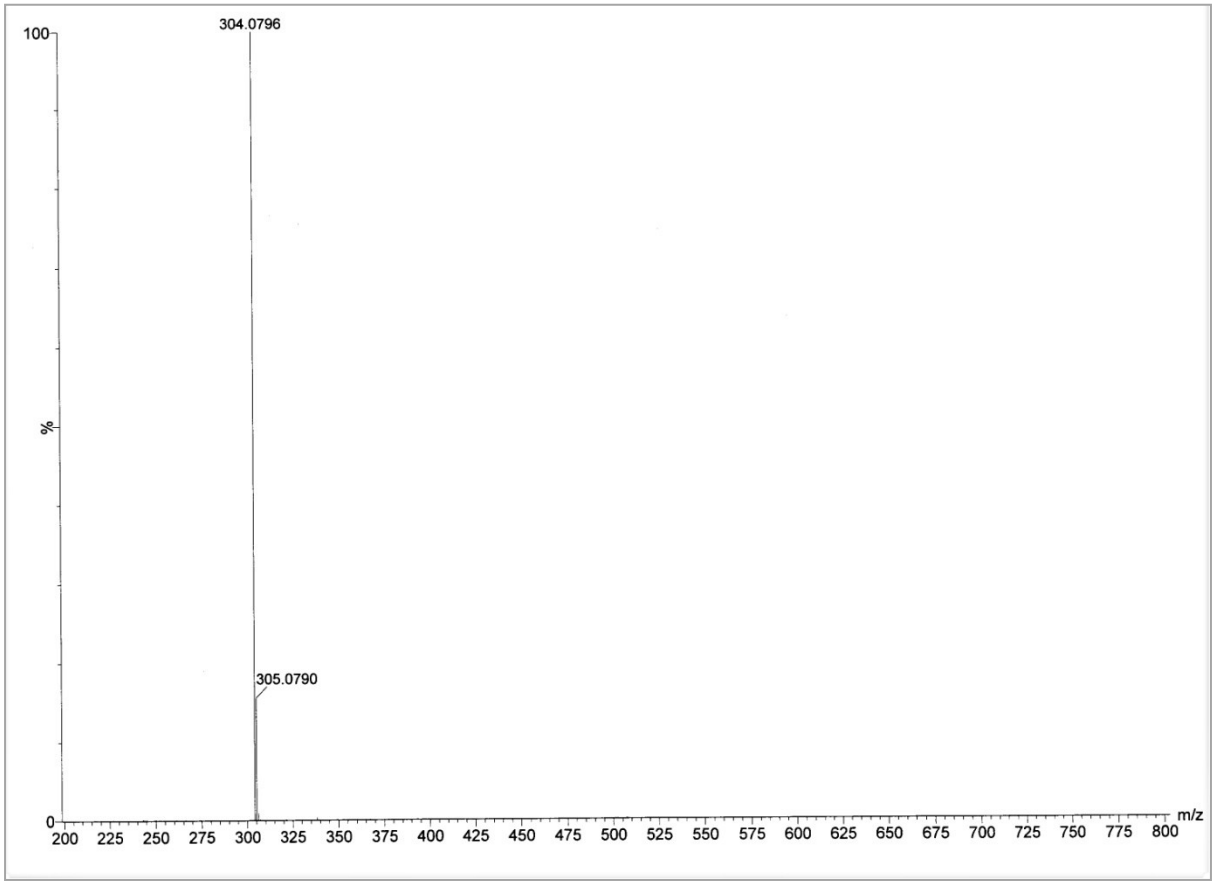

Fig. S21: HRMS of **H_2L**

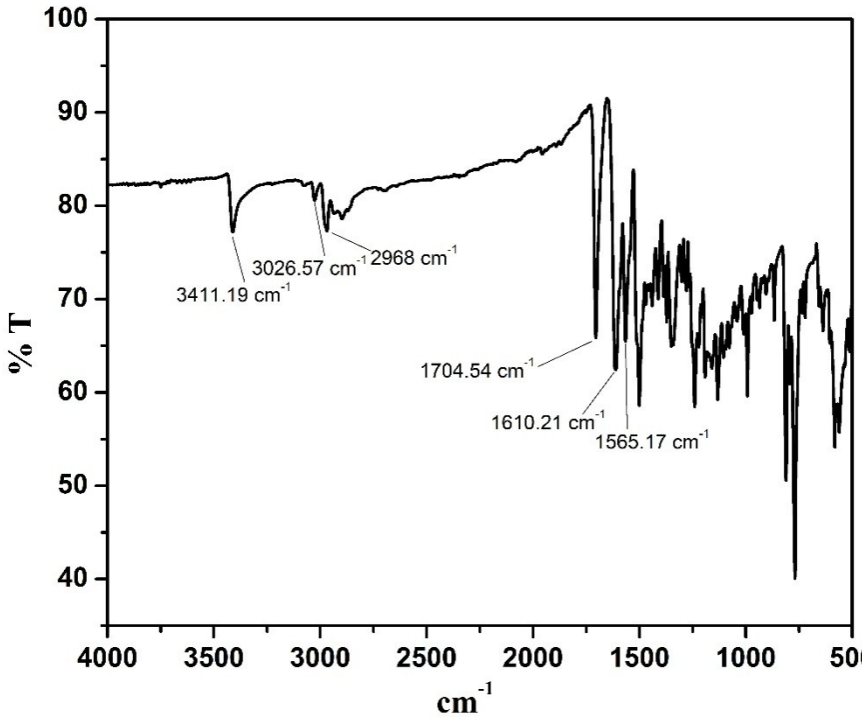

Fig. S22: IR spectra of the probe **H_2L**

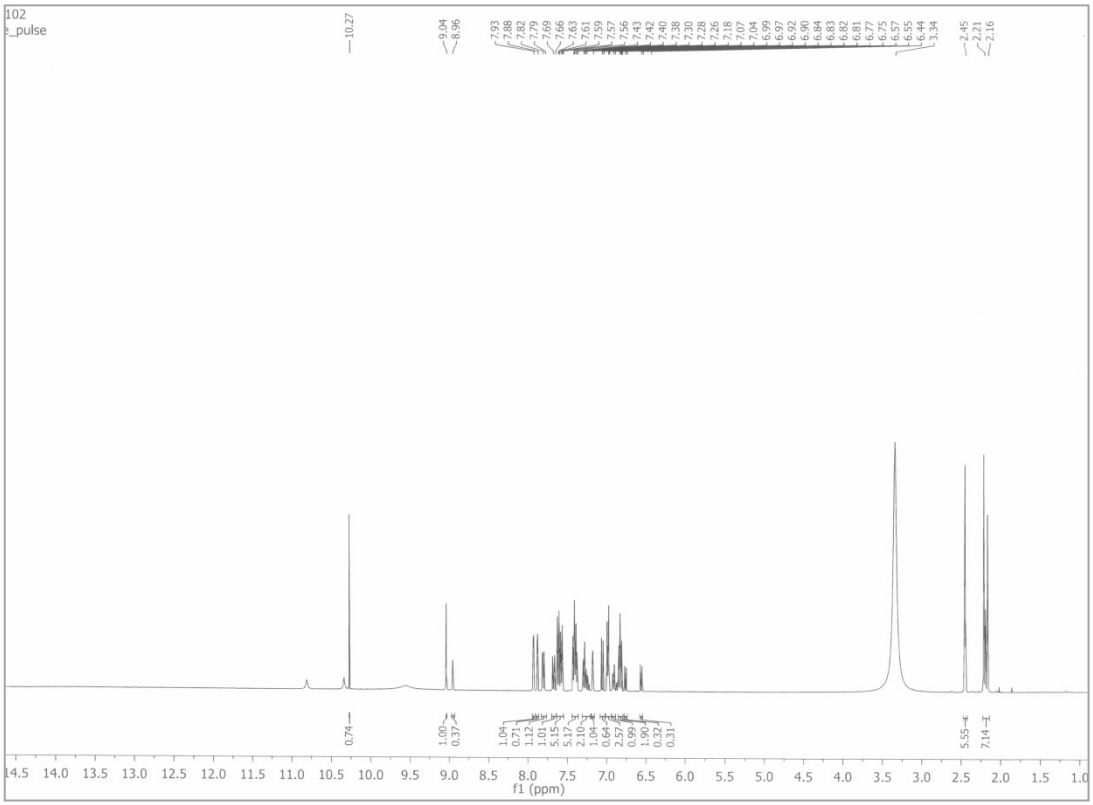

Fig.S23: ^1H NMR (400 MH_Z) spectrum of the adduct **H_2L+Al^{3+}**(1 eqiv.) in DMSO-d_6

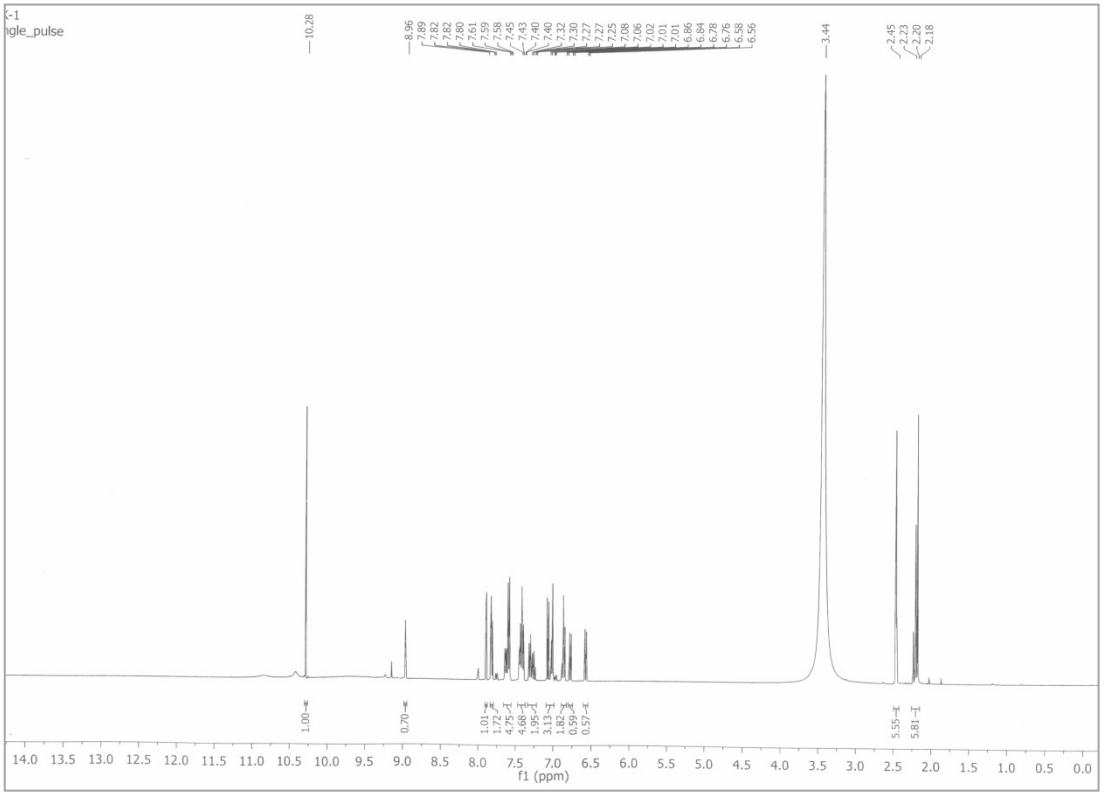

Fig.S24:^{1}H NMR (400 MH_Z) spectrum of the adduct $\mathbf{H_2L}$+$\mathbf{Al^{3+}}$(2 eqiv.) in DMSO-d_6

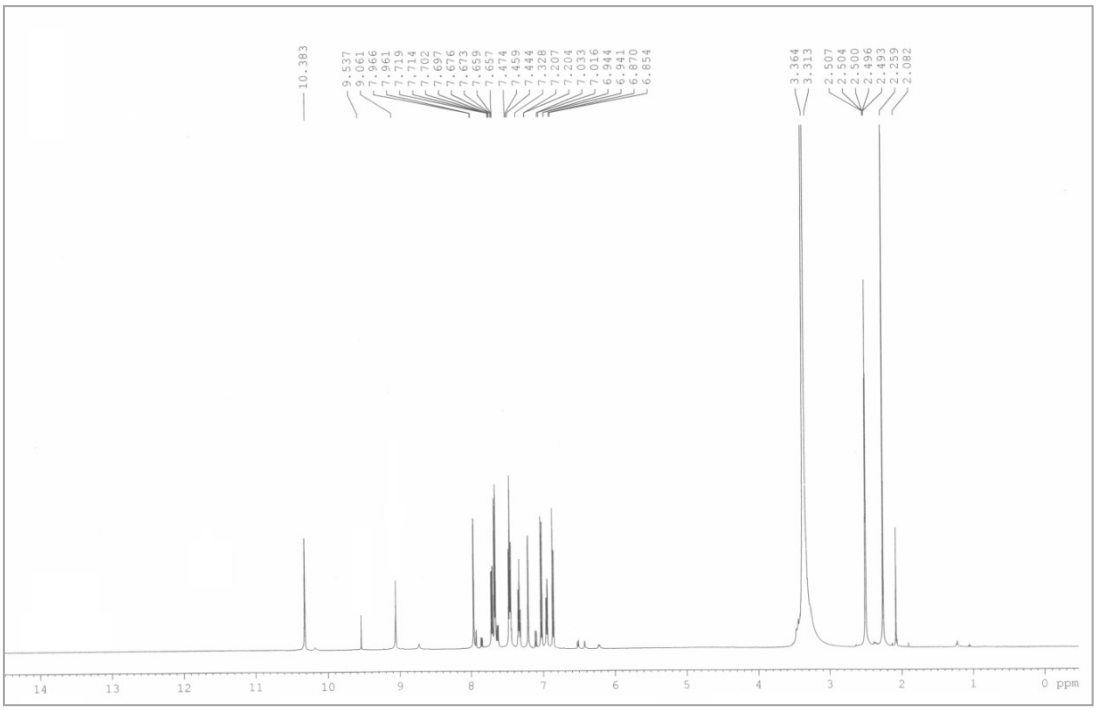

Fig.S25:^{1}H NMR (400 MH_Z) spectrum of the adduct $\mathbf{H_2L}$+$\mathbf{Zn^{2+}}$(1 eqiv.) in DMSO-d_6.

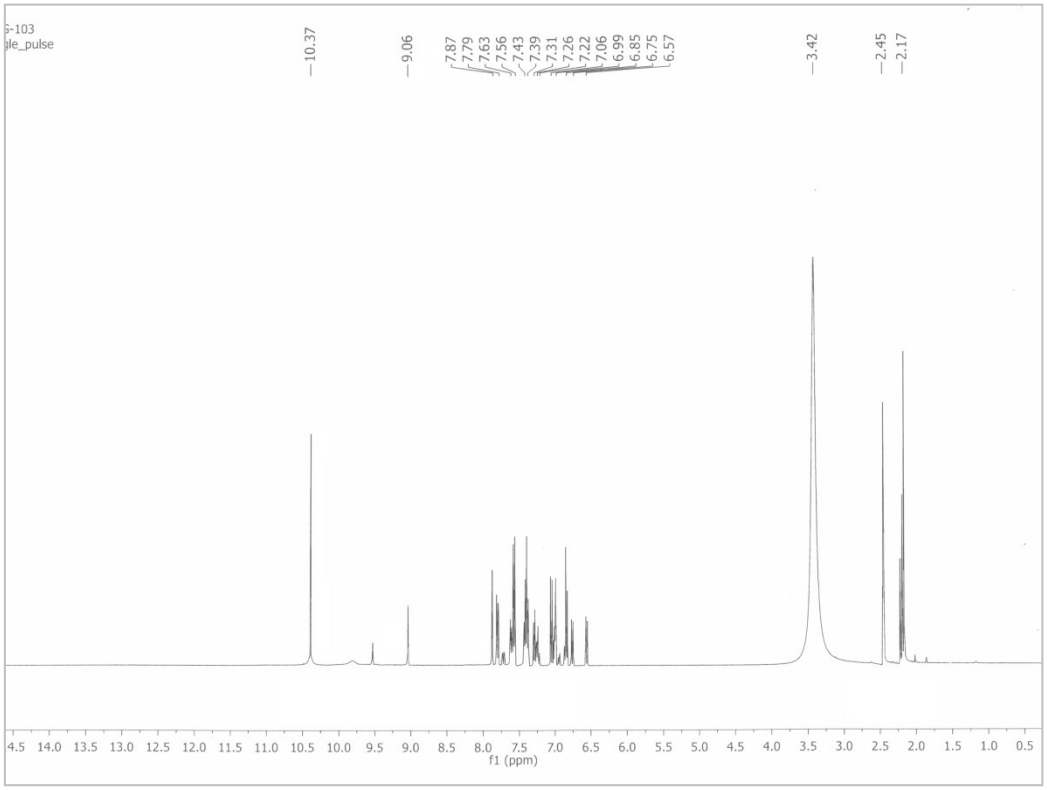

Fig.S26:[1]H NMR (400 MH_Z) spectrum of the adduct $\mathbf{H_2L+Zn^{2+}}$(2 eqiv.) in DMSO-d_6.

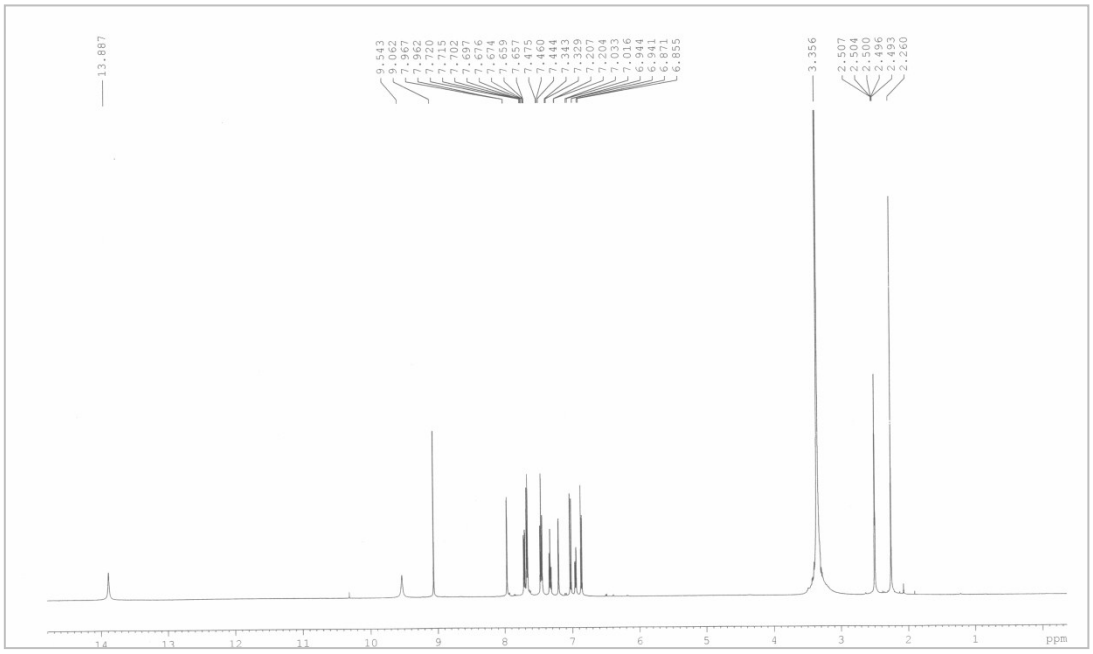

Fig.S27:[1]H NMR (400 MH_Z) spectrum of the adduct $\mathbf{H_2L+F^-}$(1 equ.) in DMSO-d_6.

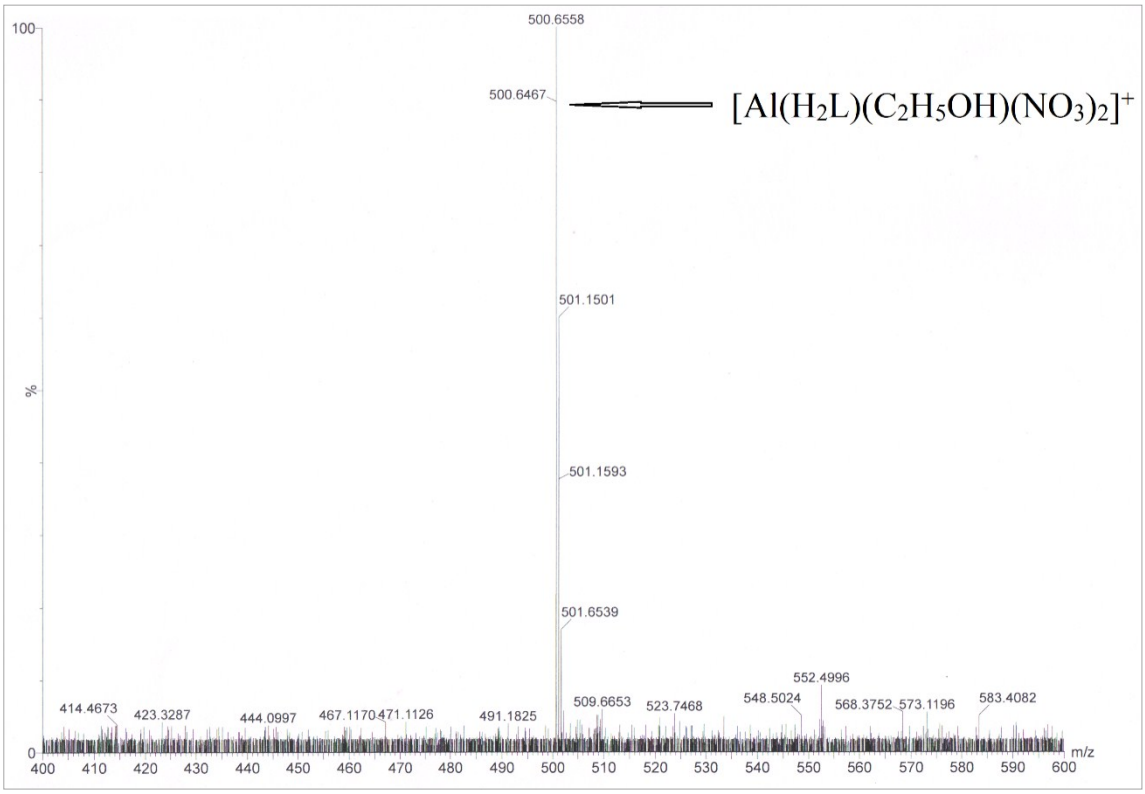

Fig. S28: HRMS of the **H_2L-Al^{3+}**complex.

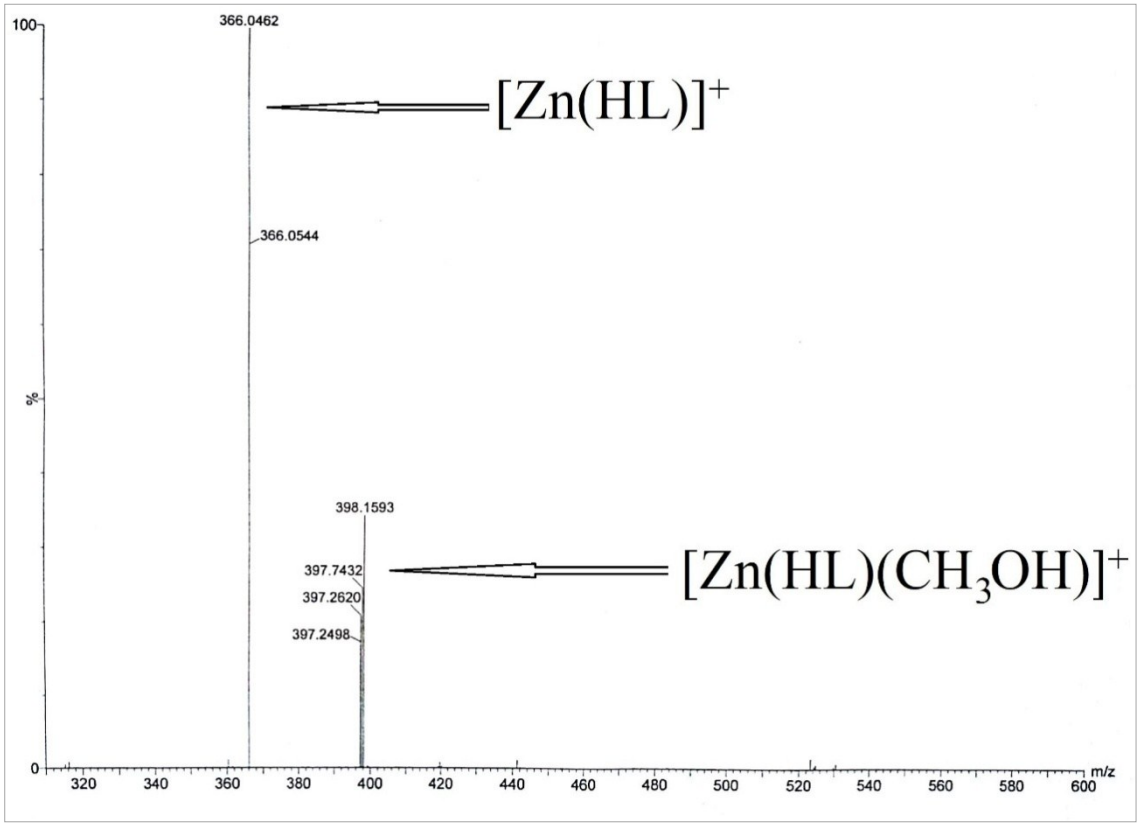

Fig. S29: HRMS of the **H_2L-Zn^{2+}** complex.

Computational study

Full geometry optimizations were carried out using the density functional theory (DFT) method at the B3LYP[1] level for the compounds. All elements except Zn and Al were assigned 6-31+G(d) basis set. The LanL2DZ basis set with effective core potential (ECP) set of Hay and Wadt[2] was used for both Zn and Al. The vibrational frequency calculations were performed to ensure that the optimized geometries represent the local minima and there were only positive eigen values. Vertical electronic excitations based on B3LYP optimized geometries were computed using the time-dependent density functional theory (TDDFT) formalism[3] in methanol using conductor like polarizable continuum model (CPCM).[4] All calculations were performed with Gaussian09 program package[5] with the aid of the GaussView visualization program.

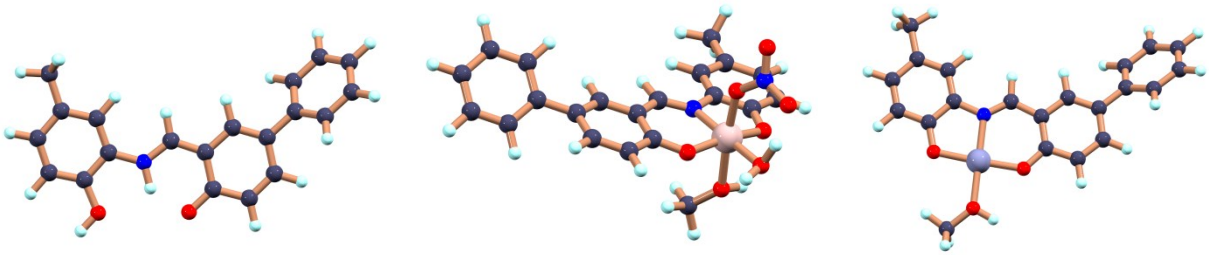

A **B** **C**

Fig. S30: Optimized structure of receptor H_2L, H_2L-Al^{3+} and H_2L-Zn^{2+} complexes

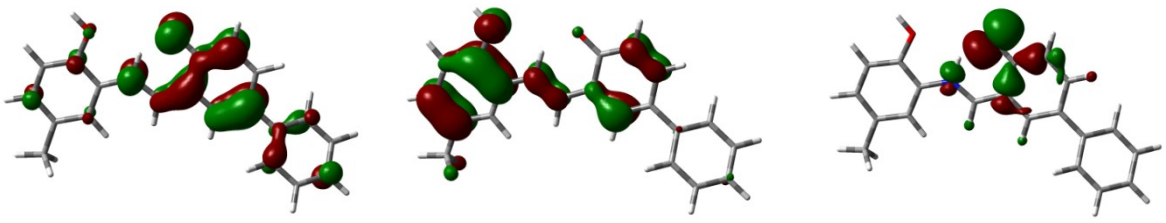

HOMO (E, -5.34 eV) HOMO-1 (E, -6.42 eV) HOMO-2 (E, -6.48 eV)

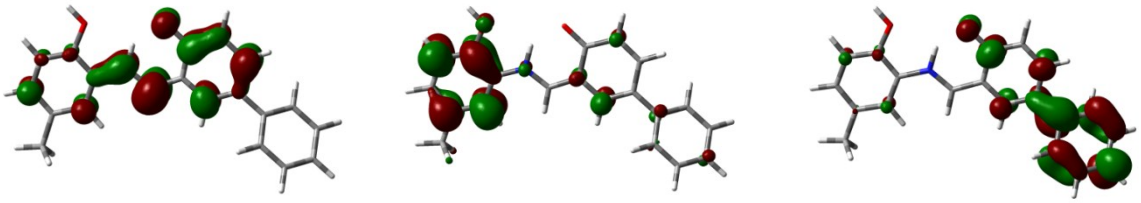

LUMO (E, -2.36 eV) LUMO+1 (E, -0.71 eV) LUMO+2 (E, -0.65 eV)

Fig. S31: Contour plots of selected molecular orbitals of receptor H_2L

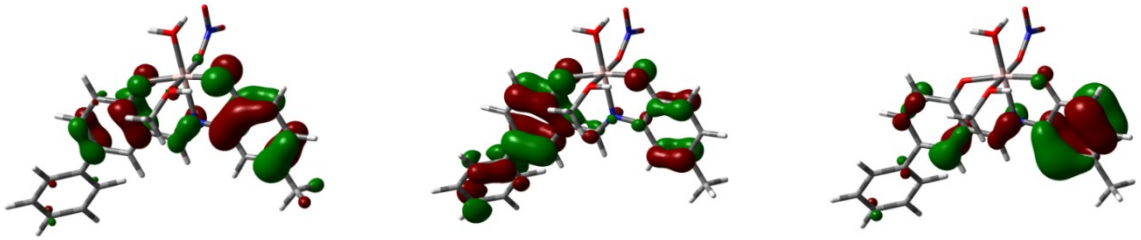

HOMO (E, -5.32eV) HOMO-1 (E, -5.81 eV) HOMO-2 (E, -6.48 eV)

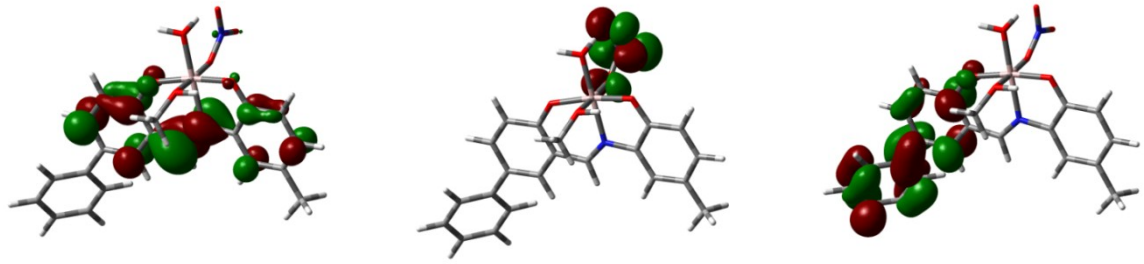

LUMO (E, -2.1 eV) LUMO+1 (E, -0.93 eV) LUMO+2 (E, -0.64 eV)

Fig. S32: Contour plots of selected molecular orbitals of **H_2L-Al^{3+}** complex

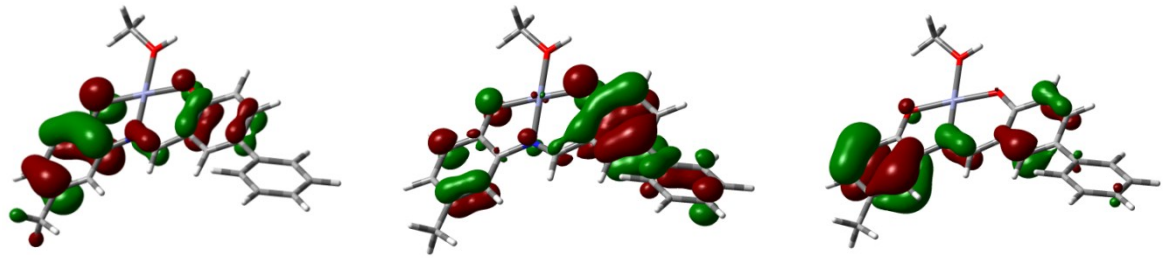

HOMO (E, -4.83 eV) HOMO-1 (E, -5.33 eV) HOMO-2 (E, -6.03 eV)

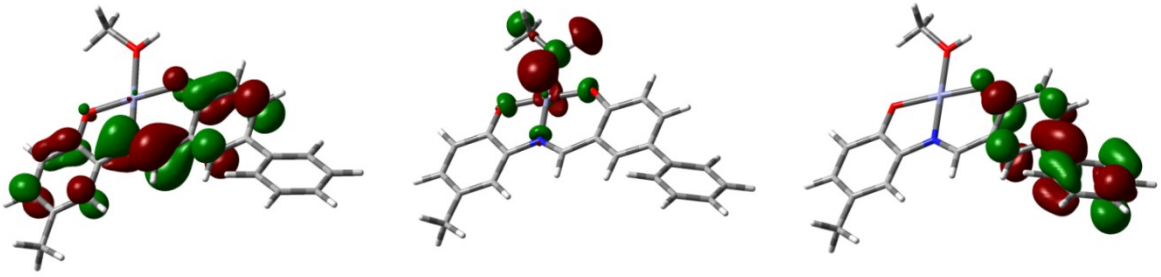

LUMO (E, -1.59 eV) LUMO+1 (E, -0.6 eV) LUMO+2 (E, -0.35 eV)

Fig. S33: Contour plots of selected molecular orbitals of **H_2L-Zn^{2+}** complex

Table S2: Vertical electronic transitions of H_2L, H_2L-Al^{3+} and H_2L-Zn^{2+} calculated by TDDFT/CPCM method

Compds.	λ (nm)	E (eV)	Osc. Strength (f)	Key excitations	$\lambda_{expt.}$ (nm)
H_2L	459.9	2.6957	0.4336	(99%)HOMO→LUMO	467
	368.0	3.3689	0.2186	(97%)HOMO-1→LUMO	359
H_2L-Al^{3+}	433.1	2.8627	0.3454	(97%)HOMO→LUMO	431
	339.09	3.6564	0.4643	(96%)HOMO-2→LUMO	352
H_2L-Zn^{2+}	436.90	2.8378	0.5040	(98%)HOMO→LUMO	432
	379.4	3.2676	0.0458	(96%)HOMO-1→LUMO	356

X-ray crystallography

Single crystals of H_2L were obtained by slow diffusion of *n*-hexane into dichloromethane solution of the complex. X-ray data were collected using an automated Bruker AXS Kappa smart Apex-II diffractometer equipped with an Apex-II CCD area detector using a fine focus sealed tube as the radiation source of graphite monochromated Mo Kα radiation (λ = 0.71073

Å). Details of crystal analyses, data collection and structure refinement are summarized in Table S3. Reflection data were recorded using the ω scan technique. The structure was solved by SHELXL-2016/6[6] and refined by full matrix least squares method. The absorption corrections were done by multi-scan (SHELXTL program package) and all the data were corrected for Lorentz, polarization effect. Hydrogen atoms were included in the refinement process as per the riding model. The crystallographic data have been deposited to the Cambridge Crystallographic Data Center: Deposition numbers CCDC 1851659.

Table S3: Crystallographic data and refinement parameters of H_2L

Formula	$C_{20}\ H_{17}\ N\ O_2$
Formula Weight	303.35
Crystal System	*Orthorhombic*
Space group	*$Pca2_1$*
a, b, c [Å]	13.8678(10), 13.8895(10), 8.3340(6)
α	90
β	90
γ	90
V [$Å^3$]	1605.3(2)
Z	4
D(calc) [g/cm^3]	1.255
μ (Mo Kα) [mm^{-1}]	0.081
F(000)	640
Absorption Correction	*multi-scan*
Temperature (K)	293(2)
Radiation [Å]	0.71073

θ(Min-Max) [º]	2.075- 25.643
Dataset (h; k; l)	-16 and 16; -16 and 16; -10 and 10
Total, Unique Data, R(int)	17077/2937/0.0622
Observed data [I > 2σ(I)]	2143
Nref, Npar	2937/216
R, wR_2	0.0493, 0.1314
Δq(max) and Δq(min) [e/Å^3]	0.143 and -0.170
Goodness of fit(S)	0.995

Table S4. Comparison of solvent systems and limit of detection (LOD) of the receptor (H_2L) with some reported fluorescence organic probes for the detection of Al^{3+} and Zn^{2+}

Receptor	Solvent system	Detection limit		Reference
		Al^{3+}	Zn^{2+}	
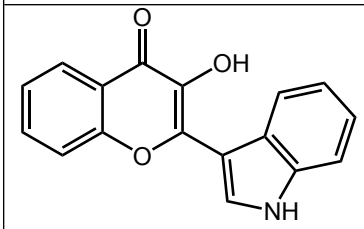	CH_3OH-H_2O (9/1,v/v)	0.62×10^{-7} M	1.67×10^{-7} M	*Sens. Actuators B*, 2017, **241**, 1090–1098.
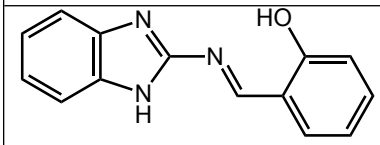	DMSO for Al^{3+} , CH_3OH for Zn^{2+}	5.26×10^{-6} M	5.98×10^{-6} M	*Inorg. Chem.*, 2014, **53**, 3012−3021
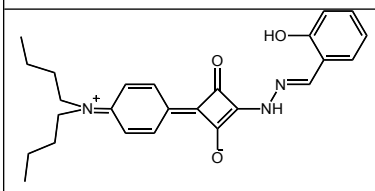	C_2H_5OH-H_2O (9/1,v/v)	1.77×10^{-7} M	2.13×10^{-8} M	*Sens. Actuators B*, 2017, **249**, 386–394.
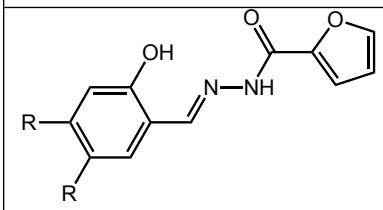	1% DMSO in H_2O	3.1×10^{-9} M	-	*ACS Sens.*, 2016, **1**, 144−150.
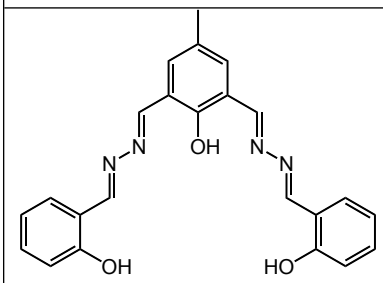	C_2H_5OH-H_2O (1/1,v/v)	6.8×10^{-8} M	5.7×10^{-8} M	*ACS Sens.*, 2016, **1**, 81−87.
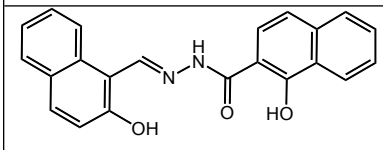	DMSO-H_2O (9/1,v/v)	3.66×10^{-6} M	1.01×10^{-6} M	*Sens. Actuators B*, 2017, **244**, 914–921
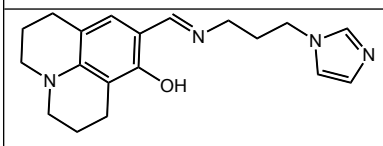	H_2O-CH_3CN (1:9, v/v)	3.9×10^{-6} M	15.6×10^{-6} M	*Sens. Actuators B*, 2014, **194**, 343–352.
This work	CH_3OH-H_2O (4/1,v/v)	2.24×10^{-7} M	4.1×10^{-8} M	

Reference

1. (a) A. D. Becke, *J. Chem. Phys.*, 1993, **98**, 5648-5652; (b) C. Lee, W. Yang, R. G. Parr, *Phys. Rev. B*, 1988, **37**, 785-789.

2. P. J. Hay and W. R. Wadt, *J. Chem. Phys.*, 1985, **82**, 299.

3. (a) R. Bauernschmitt and R. Ahlrichs, *Chem. Phys. Lett.* 1996, **256**, 454. (b) R.E. Stratmann, G.E. Scuseria and M.J. Frisch, *J. Chem. Phys.* 1998, **109**, 8218. (c) M.E. Casida, C. Jamorski, K.C. Casida and D.R. Salahub, *J. Chem. Phys.* 1998, **108**, 4439.

4. a) V. Barone and M. Cossi, *J. Phys. Chem. A* 1998, **102**, 1995; (b) M. Cossi and V. Barone, *J. Chem. Phys.* 2001, **115**, 4708; (c) M. Cossi, N. Rega, G. Scalmani and V. Barone, *J. Comput. Chem*. 2003, **24**, 669.

5. Gaussian 09, Revision D.01, M. J. Frisch, G. W. Trucks, H. B. Schlegel, G. E. Scuseria, M. A. Robb, J. R. Cheeseman, G. Scalmani, V. Barone, B. Mennucci, G. A. Petersson, H. Nakatsuji, M. Caricato, X. Li, H. P. Hratchian, A. F. Izmaylov, J. Bloino, G. Zheng, J. L. Sonnenberg, M. Hada, M. Ehara, K. Toyota, R. Fukuda, J. Hasegawa, M. Ishida, T. Nakajima, Y. Honda, O. Kitao, H. Nakai, T. Vreven, J. A. Montgomery, Jr., J. E. Peralta, F. Ogliaro, M. Bearpark, J. J. Heyd, E. Brothers, K. N. Kudin, V. N. Staroverov, R. Kobayashi, J. Normand, K. Raghavachari, A. Rendell, J. C. Burant, S. S. Iyengar, J. Tomasi, M. Cossi, N. Rega, J. M. Millam, M. Klene, J. E. Knox, J. B. Cross, V. Bakken, C. Adamo, J. Jaramillo, R. Gomperts, R. E. Stratmann, O. Yazyev, A. J. Austin, R. Cammi, C. Pomelli, J. W. Ochterski, R. L. Martin, K. Morokuma, V. G. Zakrzewski, G. A. Voth, P. Salvador, J. J. Dannenberg, S. Dapprich, A. D. Daniels, Ö. Farkas, J. B. Foresman, J. V. Ortiz, J. Cioslowski and D. J. Fox, Gaussian, Inc., Wallingford CT, 2009.

6. (a) G. M. Sheldrick, *Acta Cryst.* 2008, **A64**, 112-122; (b) G. M. Sheldrick, *Acta Cryst.* 2015, **C71**, 3-8.